Substantially Enhancing Quantum Coherence of Electrons in Graphene via Electron-Plasmon Coupling

Guanghui Cheng,[1,2] Wei Qin,[1] Meng-Hsien Lin,[3] Laiming Wei,[1,2,†] Xiaodong Fan,[1,2] Huayang Zhang,[1,2] Shangjr Gwo,[3,4] Changgan Zeng,[1,2,*] J. G. Hou,[1] and Zhenyu Zhang[1]

[1]*International Center for Quantum Design of Functional Materials (ICQD), Hefei National Laboratory for Physical Sciences at the Microscale, and Synergetic Innovation Center of Quantum Information and Quantum Physics, University of Science and Technology of China, Hefei, Anhui 230026, China*

[2]*CAS Key Laboratory of Strongly-Coupled Quantum Matter Physics, and Department of Physics, University of Science and Technology of China, Hefei, Anhui 230026, China*

[3]*Department of Physics, National Tsing-Hua University, Hsinchu 30013, Taiwan*

[4]*National Synchrotron Radiation Research Center, Hsinchu 30076, Taiwan*

(Received 11 April 2017; revised manuscript received 4 August 2017; published 13 October 2017)

The interplays between different quasiparticles in solids lay the foundation for a wide spectrum of intriguing quantum effects, yet how the collective plasmon excitations affect the quantum transport of electrons remains largely unexplored. Here we provide the first demonstration that when the electron-plasmon coupling is introduced, the quantum coherence of electrons in graphene is substantially enhanced with the quantum coherence length almost tripled. We further develop a microscopic model to interpret the striking observations, emphasizing the vital role of the graphene plasmons in suppressing electron-electron dephasing. The novel and transformative concept of plasmon-enhanced quantum coherence sheds new insight into interquasiparticle interactions, and further extends a new dimension to exploit nontrivial quantum phenomena and devices in solid systems.

DOI: 10.1103/PhysRevLett.119.156803

When electrons move in solids, they interact with other diversified quasiparticles, and these essential many-body couplings modify the behaviors of electrons substantially. For example, phonon or spin fluctuation mediated electron pairing leads to superconductivity [1–3]. Polarons protect carriers from scattering with charged defects and optical phonons in hybrid organic-inorganic perovskites [4]. Plasmons, the harmonic oscillations of conduction electrons with a coherent phase, may also affect the quantum behavior of electrons. In particular, it has been revealed that the electron-plasmon coupling results in the formation of a new composite quasiparticle, i.e., plasmaron [5–7]. Nevertheless, how plasmon excitations tune the quantum transport of electrons in solids still remains to be established.

On the other hand, it was found that quantum entanglement survives during photon-plasmon-photon conversion [8,9], which strongly suggests that the quantum nature of the plasmons ensures high quantum fidelity even though a single plasmon mode already involves a massive number of electrons [8,10]. A natural question arises: Will plasmons affect the quantum behaviors of electrons in a conceptually similar, or different, manner? Here we exploit the weak localization effect in graphene [11,12], a direct measure of the constructive quantum interference of the electrons [11–14], to address this fundamental issue, and discover that electron-plasmon coupling can indeed improve the coherent quantum characteristics in graphene substantially.

Plasmons cannot be directly excited in a pristine graphene sheet by far-field light illumination due to momentum mismatch [15]. In the present study, plasmons were instead induced in graphene by nanocavity coupling [16–21] from proximal Au nanoparticles (AuNPs) synthesized using an established approach [22] (see more details in Secs. I and IIIA of Supplemental Material (SM) [23]). The AuNPs/Al_2O_3/graphene devices were then fabricated as depicted in Fig. 1. The Al_2O_3 layer is about 2 nm thick to prevent charge transfer [39] between the AuNPs and graphene. Figure 1(d) shows the optical absorption spectra of the AuNPs, and a strong plasmon resonance is featured at ~550 nm.

Next we study how the plasmon excitation in the AuNPs manipulates the quantum transport in graphene. Figure 2(a) displays the relative conductivity $[\Delta\sigma = \sigma(B) - \sigma(0)]$ of graphene as a function of magnetic field (B) at temperature (T) of 1.5 K and gate voltage of 10 V, under laser illumination with a wavelength of 532 nm close to the AuNP plasmon resonance. Weak localization effect manifested as a dip around zero field in the $\Delta\sigma$-B curve [40–42] is featured for all the cases, arising from the constructive quantum interference of electron waves, which is gradually suppressed by the magnetic field (see more descriptions in Sec. IIA of SM [23]). Strikingly, compared to the case without illumination, the weak localization magnitude rises when the illumination is on and further increases drastically with increasing illumination power (P).

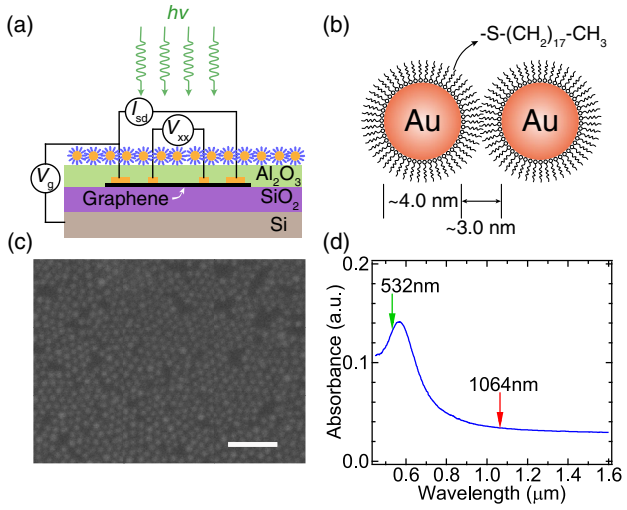

FIG. 1. Device schematics and characterizations. (a) Schematic of the AuNPs/Al_2O_3/graphene device used in the transport measurements under laser illumination. (b) Schematic of the AuNPs capped with 1-octadecanethiolate protection layer. (c) Scanning electron microscope image of a representative device. The scale bar is 40 nm. (d) Optical absorption spectra of the AuNPs on a quartz substrate.

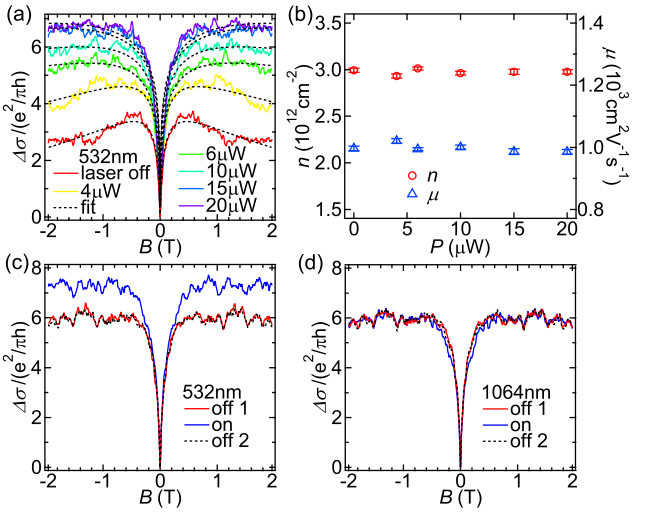

FIG. 2. Enhanced weak localization effect by plasmon excitation. (a) Relative conductivity $\Delta\sigma = \sigma(B) - \sigma(0)$ as a function of the magnetic field B for a specific device under 532-nm illumination with various powers. The dashed curves are the weak localization fittings. (b) Carrier density n and mobility μ versus laser power P. (c) $\Delta\sigma$ as a function of B for another device within an off-on-off cycle of 532-nm illumination. (d) $\Delta\sigma$ as a function of B within an off-on-off cycle of 1064-nm illumination. The photon flux in (c) and (d) is the same ($\sim 1 \times 10^{11}$ s^{-1} mm^{-2}).

We then discuss the likely mechanisms leading to such drastically enhanced weak localization effect. It could be induced by changes in the carrier density (n) and mobility (μ) of graphene [40,41] upon illumination. However, the variations of n and μ in response to laser illumination are too weak [<4% as shown in Fig. 2(b)] to account for the giant increase of the weak localization magnitude. Another possibility might be attributed to the effect of the applied electromagnetic field on the graphene. However, such a field effect was revealed to offer an additional dephasing channel to suppress weak localization [43–45]. A third possible factor could be the overheating of graphene electrons caused by the illumination. However, if such a thermal effect played a dominant role, the weak localization magnitude would decrease with increasing laser power [13,46], contrary to the revealed behaviors.

Based on the discussions above, the enhanced weak localization effect in graphene can most probably be attributed to the effect of the plasmon excitations in the proximal AuNPs. To further validate the plasmonic origin, magnetotransport was further performed under illumination with different wavelengths but the same photon flux. For 532-nm illumination, weak localization is enhanced notably and returns to the initial state after removal of the illumination [Fig. 2(c)]. This suggests that the weak localization enhancement is a pure electronic effect without irreversible atomic reconstruction. In sharp contrast, the weak localization under 1064-nm illumination is almost the same as that without illumination [Fig. 2(d)], which can be attributed to the fact that this wavelength is far away from the AuNP plasmon resonance. Moreover, no weak localization enhancement is observed for the bare Al_2O_3/graphene/SiO_2/Si or graphene/SiO_2/Si samples under 532-nm illumination (see Fig. S2 in SM [23]). These control experiments confirm unambiguously that the enhanced weak localization effect in graphene must arise from the plasmonic effect of the proximal AuNPs.

Because the weak localization magnitude is largely determined by the phase coherence length [13,47], our observation strongly suggests that the quantum coherence in the graphene in proximity to the AuNPs is drastically enhanced under laser illumination. To quantitatively characterize this effect, the measured magnetoconductivities in Fig. 2(a) were fitted using the well-established formalism adopted to describe weak localization effects in graphene [11,40,42],

$$\Delta\sigma(B) = \frac{e^2}{\pi h}\left[F\left(\frac{B}{B_\phi}\right) - F\left(\frac{B}{B_\phi + 2B_i}\right) - 2F\left(\frac{B}{B_\phi + B_i + B_*}\right)\right],$$

where $F(z) = \ln(z) + \Psi(1/2 + z^{-1})$, $\Psi(x)$ is the digamma function, and $B_{\phi,i,*} = \hbar/(4eL^2_{\phi,i,*})$. Here L_ϕ is the phase coherence length above which the coherence is lost due to inelastic scatterings, L_i the elastic intervalley scattering length, and L_* the elastic intravalley scattering length. The dephasing rate (τ_ϕ^{-1}) can be extracted from the relation $\tau_\phi^{-1} = D/L_\phi^2$, where $D = V_F^2\tau_{\rm tr}/2$ denotes the diffusion

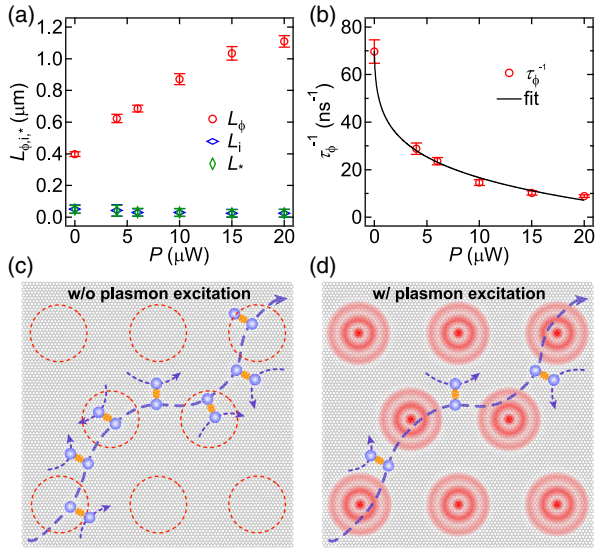

FIG. 3. Plasmon-enhanced quantum coherence and the mechanism. (a) Phase coherence length L_ϕ, elastic intervalley scattering length L_i, and elastic intravalley scattering length L_* as functions of 532-nm laser power P, extracted from the weak localization fittings in Fig. 2(a). (b) Extracted dephasing rate τ_ϕ^{-1} as a function of P. The black curve is the fitting based on the phenomenological model described in Sec. III of SM [23]. (c) Schematic of an electron trajectory (blue curve) in graphene without plasmon excitation. The pairs of blue balls with yellow ties represent inelastic electron-electron scattering events that break the phase coherence. The red dotted circles indicate the unexcited plasmon domains underneath the AuNPs. (d) Schematic of an electron trajectory with plasmon excitation. The red shaded concentric circles are domains of plasmon excitation, in which the inelastic scattering is suppressed.

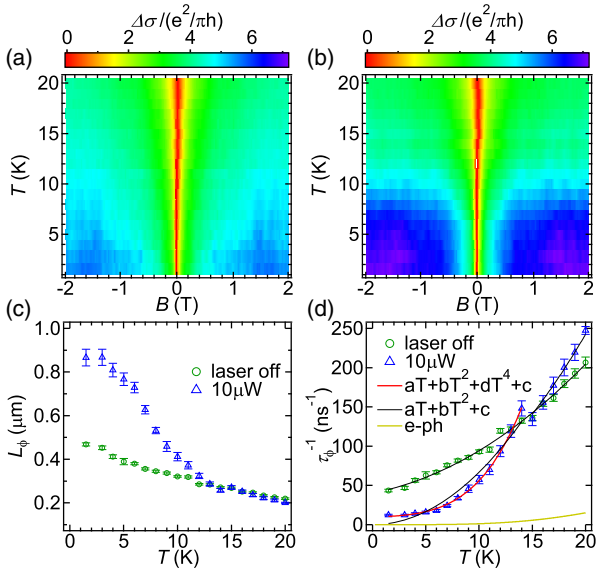

FIG. 4. Temperature dependence of plasmon-enhanced quantum coherence. (a) T-dependent weak localization effect for a third device without illumination. (b) T-dependent weak localization effect with 532-nm laser illumination. (c) Extracted phase coherence length L_ϕ as a function of T without and with 532-nm illumination. (d) Extracted dephasing rate τ_ϕ^{-1} as a function of T. Fittings and calculation by adopting various models are also shown.

coefficient, $V_F \approx 1.1 \times 10^6$ m/s the Fermi velocity [48,49], and $\tau_{\rm tr} = \mu\hbar\sqrt{\pi n}/(eV_F)$ the momentum relaxation time.

As displayed in Fig. 2(a), the weak localization data can be well fitted within this formalism. The derived L_ϕ, L_i, L_*, and τ_ϕ^{-1} as functions of P are plotted in Figs. 3(a) and 3(b), respectively. It is evident that L_ϕ (τ_ϕ^{-1}) rises (drops) dramatically with increasing P, with L_ϕ varying from ~400 nm at 0 μW to ~1100 nm at 20 μW. Meanwhile, L_i decreases from ~50 to ~25 nm. Although the enhanced intervalley scattering may contribute to the weak localization enhancement [11,50,51], the increase in L_ϕ plays a critical role in enhancing the weak localization under resonant illumination, as detailed in Sec. IIB of SM [23].

It is noted that the universal conductance fluctuations (UCF), manifested as reproducible fluctuations in the $\Delta\sigma$-B curves [12,40], do not show a clear increasing amplitude upon increasing the illumination power (see Fig. 2 and Fig. S4 in SM [23]). As detailed in Sec. IIC of SM [23], the UCF magnitude in the present case depends not only on L_ϕ, but also on the thermal length L_T, L_i, and L_* [52–55]. Qualitatively, the decrease in L_i, L_*, and L_T upon resonant illumination would suppress the UCF [52–55]; therefore, the increase in L_ϕ may not necessarily lead to a clear enhancement in the UCF magnitude.

The dependence of the plasmonic origin on temperature is further exploited in the low-temperature regime without and with 532-nm illumination, respectively, as shown in Figs. 4(a) and 4(b). It is evident that the enhancement of quantum coherence disappears above 13 K, which is more obvious from the derived T-dependent L_ϕ and τ_ϕ^{-1} as displayed in Figs. 4(c) and 4(d).

The dominant dephasing mechanism can be inferred from the T dependence of τ_ϕ^{-1} [13,40–42,56]. As revealed in Fig. 4(d), in the absence of plasmon excitation, $\tau_\phi^{-1}(T)$ can be well fitted by the conventional electron-electron dephasing mechanism [40,42], $\tau_\phi^{-1}(T) = aT + bT^2 + c$, where the first term arises from the interaction of an electron with the fluctuating electromagnetic field induced by the noisy movement of the neighboring electrons (Nyquist dephasing) [40], while the second term arises from the direct Coulomb interaction of the electrons [40] with a, b, and c as constants. Meanwhile, the electron-phonon scattering rate ($\tau_{e-{\rm ph}}^{-1}$) estimated from the model based on the Boltzmann transport theory [57,58] is much smaller than the experimentally derived τ_ϕ^{-1}. These results demonstrate that electron-electron scattering is the dominant dephasing mechanism in graphene at low temperature, consistent with previous studies [40,41,59].

In the presence of plasmon excitations in the proximal AuNPs, the electron-electron dephasing picture can still fit

the $\tau_\phi^{-1}(T)$ behavior above 14 K. However, this picture fails to describe the $\tau_\phi^{-1}(T)$ behavior below 14 K as revealed in Fig. 4(d). Rather, the low-temperature behavior is better fitted if an additional T^4 term is taken into account [$\tau_\phi^{-1}(T) = aT + bT^2 + dT^4 + c$, d being another constant]. Such deviations further imply the critical role of plasmon coupling in enhancing quantum coherence, even though this quantum coupling effect is unable to survive at high temperatures (see more discussion in Sec. IV of SM [23]).

A microscopic phenomenological model is therefore proposed to explain the discovered plasmon-enhanced quantum coherence in graphene. With the excitation of AuNPs plasmon under laser illumination, the strong near-field couplings, namely, nanocavity modes [16–21], between the AuNPs and graphene induce plasmon excitations, i.e., simultaneous electron oscillations in graphene under the AuNPs (see more discussion in Sec. IIIA of SM [23]). As a consequence of multichannel damping, the collective plasmon excitations form two-dimensional domains centered at the AuNPs as schematically illustrated in Figs. 3(c) and 3(d). For simplicity without losing the essential physics, we adopt the scheme that the electron-plasmon interaction is mainly responsible for the inelastic scattering events when the electron trajectory passes through the plasmon excitation domains [red shaded regions in Figs. 3(c) and 3(d)], whereas the conventional electron-electron interactions contribute to the inelastic scattering events in other regions. Such a scheme is justified as detailed in Sec. IIID of SM [23]. The total dephasing rate can then be expressed as $\tau_\phi^{-1} = (1-\xi)\tau_{e-e}^{-1} + \xi\tau_{e-\mathrm{pl}}^{-1}$, where ξ (≤ 1) denotes the fractional area of the plasmon domains, $\tau_{e-\mathrm{pl}}^{-1}$ the electron-plasmon scattering rate, and τ_{e-e}^{-1} the electron-electron scattering rate. As theoretically analyzed in detail in Secs. IIIB and IIIC of SM [23], $\tau_{e-\mathrm{pl}}^{-1}$ is much lower than τ_{e-e}^{-1}. Consequently, the total inelastic scattering is effectively suppressed, leading to the enhancement of quantum coherence.

At a deeper level, plasmons as the collective excitations of electrons arise from the long-range Coulomb interaction of the electrons. Although the estimated lifetime of plasmon in the present system is quite short, the persistent and stable laser illumination drives such a system into a dynamically equilibrium state, where the collective plasmonic excitations can effectively define the steady plasmon domains (see detailed discussion in Sec. IIIC of SM [23]). Furthermore, the excitation of plasmon domains enhances the effectiveness of screening, which in turn largely exhausts the long-range component of the Coulomb interaction. This makes the constituent electrons of plasmon domains invisible for transporting electrons, which consequently reduce the electron-electron scattering rate.

The dependence of the plasmon-enhanced quantum coherence on the illumination power can be well interpreted within this phenomenological model. Under laser illumination, the size of the plasmon domains gradually increases with increasing P (see more details in Sec. IIID and Fig. S5 in SM [23]); consequently, τ_ϕ^{-1} decreases continuously until the plasmon domains cover nearly the whole area of the graphene layer. Figure 3(b) shows that the phenomenological model fits the experimentally obtained $\tau_\phi^{-1}(P)$ very well (see more details in Sec. IIID of SM [23]).

The present study has demonstrated the vital role of electron-plasmon coupling in enhancing quantum coherence of electrons in solids. This conceptual discovery, in principle, paves the way to the realization of nontrivial quantum effects by tailoring the delicate coupling between quantum quasiparticles. For example, the revealed strong electron-plasmon coupling may eventually stabilize plasmon-mediated superconductivity [60]. Moreover, the drastically enhanced quantum fidelity by electron-plasmon coupling may promise versatile quantum device applications, especially for quantum computing [61].

We thank Xiaoguang Li for helpful discussion. This work was supported in part by the National Basic Research Program of China (Grant No. 2014CB921102), National Key R&D Program of China (Grant No. 2017YFA0403600), National Natural Science Foundation of China (Grants No. 11434009, No. 11374279, No. 11461161009, No. 11634011, No. 61434002, and No. 11304299), Ministry of Science and Technology in Taiwan (MOST Grant No. 105-2112-M-007-011-MY3), the Strategic Priority Research Program (B) of the Chinese Academy of Sciences (Grant No. XDB01020000), the Fundamental Research Funds for the Central Universities (Grant No. WK2030020027), and Anhui Provincial Natural Science Foundation (Grant No. 1708085MF136).

G. C., W. Q., and M.-H. L. contributed equally to this work.

*Corresponding author.
cgzeng@ustc.edu.cn
†Corresponding author.
laiming@ustc.edu.cn

[1] J. Bardeen, L. N. Cooper, and J. R. Schrieffer, Theory of superconductivity, Phys. Rev. **108**, 1175 (1957).
[2] T. Moriya, Y. Takahashi, and K. Ueda, Antiferromagnetic spin fluctuations and superconductivity in two-dimensional metals—a possible model for high T_c oxides, J. Phys. Soc. Jpn. **59**, 2905 (1990).
[3] T. Dahm, V. Hinkov, S. V. Borisenko, A. A. Kordyuk, V. B. Zabolotnyy, J. Fink, B. Büchner, D. J. Scalapino, W. Hanke, and B. Keimer, Strength of the spin-fluctuation-mediated pairing interaction in a high-temperature superconductor, Nat. Phys. **5**, 217 (2009).
[4] H. Zhu, K. Miyata, Y. Fu, J. Wang, P. P. Joshi, D. Niesner, K. W. Williams, S. Jin, and X.-Y. Zhu, Screening in crystalline liquids protects energetic carriers in hybrid perovskites, Science **353**, 1409 (2016).

[5] B. I. Lundqvist, Single-particle spectrum of the degenerate electron gas: I. The structure of the spectral weight function, Phys. Kondens. Mater. **6**, 193 (1967).
[6] R. Tediosi, N. P. Armitage, E. Giannini, and D. van der Marel, Charge Carrier Interaction with a Purely Electronic Collective Mode: Plasmarons and the Infrared Response of Elemental Bismuth, Phys. Rev. Lett. **99**, 016406 (2007).
[7] A. Bostwick, F. Speck, T. Seyller, K. Horn, M. Polini, Reza Asgari, A. H. MacDonald, and E. Rotenberg, Observation of plasmarons in quasifreestanding doped graphene, Science **328**, 999 (2010).
[8] E. Altewischer, M. P. van Exter, and J. P. Woerdman, Plasmon-assisted transmission of entangled photons, Nature (London) **418**, 304 (2002).
[9] S. Fasel, F. Robin, E. Moreno, D. Erni, N. Gisin, and H. Zbinden, Energy-Time Entanglement Preservation in Plasmon-Assisted Light Transmission, Phys. Rev. Lett. **94**, 110501 (2005).
[10] M. S. Tame, K. R. McEnery, Ş. K. Özdemir, J. Lee, S. A. Maier, and M. S. Kim, Quantum plasmonics, Nat. Phys. **9**, 329 (2013).
[11] E. McCann, K. Kechedzhi, V. I. Fal'ko, H. Suzuura, T. Ando, and B. L. Altshuler, Weak-Localization Magnetoresistance and Valley Symmetry in Graphene, Phys. Rev. Lett. **97**, 146805 (2006).
[12] S. V. Morozov, K. S. Novoselov, M. I. Katsnelson, F. Schedin, L. A. Ponomarenko, D. Jiang, and A. K. Geim, Strong Suppression of Weak Localization in Graphene, Phys. Rev. Lett. **97**, 016801 (2006).
[13] G. Bergmann, Weak localization in thin films: A time-of-flight experiment with conduction electrons, Phys. Rep. **107**, 1 (1984).
[14] J. Hu, X. Liu, C. L. Yue, J. Y. Liu, H. W. Zhu, J. B. He, J. Wei, Z. Q. Mao, L. Yu. Antipina, Z. I. Popov, P. B. Sorokin, T. J. Liu, P. W. Adams, S. M. A. Radmanesh, L. Spinu, H. Ji, and D. Natelson, Enhanced electron coherence in atomically thin Nb_3SiTe_6, Nat. Phys. **11**, 471 (2015).
[15] L. Ju, B. Geng, J. Horng, C. Girit, M. Martin, Z. Hao, H. A. Bechtel, X. Liang, A. Zettl, Y. R. Shen, and F. Wang, Graphene plasmonics for tunable terahertz metamaterials, Nat. Nanotechnol. **6**, 630 (2011).
[16] R. W. Rendell, D. J. Scalapino, and B. Mühlschlegel, Role of Local Plasmon Modes in Light Emission from Small-Particle Tunnel Junctions, Phys. Rev. Lett. **41**, 1746 (1978).
[17] R. W. Rendell and D. J. Scalapino, Surface plasmons confined by microstructures on tunnel junctions, Phys. Rev. B **24**, 3276 (1981).
[18] R. Ruppin, Surface modes and optical absorption of a small sphere above a substrate, Surf. Sci. **127**, 108 (1983).
[19] P. K. Aravind and H. Metiu, The effects of the interaction between resonances in the electromagnetic response of a sphere-plane structure; applications to surface enhanced spectroscopy, Surf. Sci. **124**, 506 (1983).
[20] S. Hayashi, in *Near-Field Optics and Surface Plasmon Polaritons*, edited by S. Kawata (Springer, New York, 2001).
[21] N. J. Halas, S. Lal, W.-S. Chang, S. Link, and P. Nordlander, Plasmons in strongly coupled metallic nanostructures, Chem. Rev. **111**, 3913 (2011).
[22] C.-F. Chen, S.-D. Tzeng, H.-Y. Chen, K.-J. Lin, and S. Gwo, Tunable plasmonic response from alkanethiolate-stabilized gold nanoparticle superlattices: Evidence of near-field coupling, J. Am. Chem. Soc. **130**, 824 (2008).
[23] See Supplemental Material at http://link.aps.org/supplemental/10.1103/PhysRevLett.119.156803 for experimental and theoretical details as well as additional figures and discussions, which includes Refs. [24–38].
[24] T.-E. Bae, H. Kim, J. Jung, and W.-J. Cho, Fabrication of high-performance graphene field-effect transistor with solution-processed Al_2O_3 sensing membrane, Appl. Phys. Lett. **104**, 153506 (2014).
[25] J. Han, S. Wang, D. Qian, F. Song, X. Wang, X. Wang, B. Wang, M. Han, and J. Zhou, Room-temperature observations of the weak localization in low-mobility graphene films, J. Appl. Phys. **114**, 214502 (2013).
[26] E. H. Hwang and S. Das Sarma, Dielectric function, screening, and plasmons in two-dimensional graphene, Phys. Rev. B **75**, 205418 (2007).
[27] S. Das Sarma, S. Adam, E. H. Hwang, and E. Rossi, Electronic transport in two-dimensional graphene, Rev. Mod. Phys. **83**, 407 (2011).
[28] R. Ruppin, *Electromagnetic Surface Modes*, edited by A. D. Boardman (Wiley, Chichester, 1982), Chap. 9, pp. 345–398.
[29] J. K. Gimzewski, B. Reihl, J. H. Coombs, and R. R. Schlittler, Photon emission with the scanning tunneling microscope, Z. Phys. B **72**, 497 (1988).
[30] R. Berndt, J. K. Gimzewski, and P. Johansson, Inelastic Tunneling Excitation of Tip-Induced Plasmon Modes on Noble-Metal Surfaces, Phys. Rev. Lett. **67**, 3796 (1991).
[31] Y. Inouye, in *Near-Field Optics and Surface Plasmon Polaritons*, edited by S. Kawata (Springer, New York, 2001).
[32] Y. Liu, R. F. Willis, K. V. Emtsev, and Th. Seyller, Plasmon dispersion and damping in electrically isolated two-dimensional charge sheets, Phys. Rev. B **78**, 201403 (2008).
[33] S. In and N. Park, Inverted ultrathin organic solar cells with a quasigrating structure for efficient carrier collection and dipless visible optical absorption, Sci. Rep. **6**, 21784 (2016).
[34] A. J. Morfa, K. L. Rowlen, T. H. Reilly III, M. J. Romero, and J. van de Lagemaat, Plasmon-enhanced solar energy conversion in organic bulk heterojunction photovoltaics, Appl. Phys. Lett. **92**, 013504 (2008).
[35] V. H. Nguyen and B. H. Nguyen, Quantum dynamics of plasmons in nanomaterials, Adv. Nat. Sci. Nanosci. Nanotechnol. **3**, 035009 (2012).
[36] V. H. Nguyen and B. H. Nguyen, Basics of quantum plasmonics, Adv. Nat. Sci. Nanosci. Nanotechnol. **6**, 023001 (2015).
[37] D. S. Kainth, D. Richards, H. P. Hughes, M. Y. Simmons, and D. A. Ritchie, Temperature-dependent Landau damping of the acoustic plasmon in bilayer system, Phys. Rev. B **57**, R2065 (1998).
[38] D. S. Kainth, D. Richards, H. P. Hughes, M. Y. Simmons, and D. A. Ritchie, Electron correlations in an electron bilayer at finite temperature: Landau damping of the acoustic plasmon, J. Phys. Condens. Matter **12**, 439 (2000).
[39] A. Hoggard, L.-Y. Wang, L. Ma, Y. Fang, G. You, J. Olson, Z. Liu, W.-S. Chang, P. M. Ajayan, and S. Link, Using the plasmon linewidth to calculate the time and efficiency of

electron transfer between gold nanorods and graphene, ACS Nano **7**, 11209 (2013).
[40] D.-K. Ki, D. Jeong, J.-H. Choi, H.-J. Lee, and K.-S. Park, Inelastic scattering in a monolayer graphene sheet: A weak-localization study, Phys. Rev. B **78**, 125409 (2008).
[41] F. V. Tikhonenko, D. W. Horsell, R. V. Gorbachev, and A. K. Savchenko, Weak Localization in Graphene Flakes, Phys. Rev. Lett. **100**, 056802 (2008).
[42] X. Hong, K. Zou, B. Wang, S.-H. Cheng, and J. Zhu, Evidence for Spin-Flip Scattering and Local Moments in Dilute Fluorinated Graphene, Phys. Rev. Lett. **108**, 226602 (2012).
[43] B. L. Altshuller, A. G. Aronov, and D. E. Khmelnitsky, Suppression of localization effects by the high frequency field and the nyquist noise, Solid State Commun. **39**, 619 (1981).
[44] S. Wang and P. E. Lindelof, Microwave-Enhanced Phase-Relaxation Observed in Weak-Localization Experiments, Phys. Rev. Lett. **59**, 1156 (1987).
[45] J. Wei, S. Pereverzev, and M. E. Gershenson, Microwave-Induced Dephasing in One-Dimensional Metal Wires, Phys. Rev. Lett. **96**, 086801 (2006).
[46] R. G. Mani, J. Hankinson, C. Berger, and W. A. de Heer, Observation of resistively detected hole spin resonance and zero-field pseudospin splitting in epitaxial graphene, Nat. Commun. **3**, 996 (2012).
[47] A. M. R. Baker, J. A. Alexander-Webber, T. Altebaeumer, T. J. B. M. Janssen, A. Tzalenchuk, S. Lara-Avila, S. Kubatkin, R. Yakimova, C.-T. Lin, L.-J. Li, and R. J. Nicholas, Weak localization scattering lengths in epitaxial, and CVD graphene, Phys. Rev. B **86**, 235441 (2012).
[48] Y. Zhang, Y.-W. Tan, H. L. Stormer, and P. Kim, Experimental observation of the quantum Hall effect and Berry's phase in graphene, Nature (London) **438**, 201 (2005).
[49] D. L. Miller, K. D. Kubista, G. M. Rutter, M. Ruan, W. A. de Heer, P. N. First, and J. A. Stroscio, Observing the quantization of zero mass carriers in graphene, Science **324**, 924 (2009).
[50] A. F. Morpurgo and F. Guinea, Intervalley Scattering, Long-Range Disorder, and Effective Time-Reversal Symmetry Breaking in Graphene, Phys. Rev. Lett. **97**, 196804 (2006).
[51] B. Yan, Q. Han, Z. Jia, J. Niu, T. Cai, D. Yu, and X. Wu, Electrical control of intervalley scattering in graphene via the charge state of defects, Phys. Rev. B **93**, 041407 (2016).
[52] P. A. Lee, A. Douglas Stone, and H. Fukuyama, Universal conductance fluctuations in metals: Effects of finite temperature, interactions, and magnetic field, Phys. Rev. B **35**, 1039 (1987).
[53] G. Bergmann, Different coherence lengths in universal conductance fluctuations: A numerical calculation for the quasitwo-dimensional case, Phys. Rev. B **49**, 8377 (1994).
[54] M. Yu. Kharitonov and K. B. Efetov, Universal conductance fluctuations in graphene, Phys. Rev. B **78**, 033404 (2008).
[55] D. W. Horsell, A. K. Savchenko, F. V. Tikhonenko, K. Kechedzhi, I. V. Lerner, and V. I. Fal'ko, Mesoscopic conductance fluctuations in graphene, Solid State Commun. **149**, 1041 (2009).
[56] X. Wu, X. Li, Z. Song, C. Berger, and W. A. de Heer, Weak Antilocalization in Epitaxial Graphene: Evidence for Chiral Electrons, Phys. Rev. Lett. **98**, 136801 (2007).
[57] E. H. Hwang and S. Das Sarma, Acoustic phonon scattering limited carrier mobility in two-dimensional extrinsic graphene, Phys. Rev. B **77**, 115449 (2008).
[58] D. K. Efetov and P. Kim, Controlling Electron-Phonon Interactions in Graphene at Ultrahigh Carrier Densities, Phys. Rev. Lett. **105**, 256805 (2010).
[59] F. V. Tikhonenko, A. A. Kozikov, A. K. Savchenko, and R. V. Gorbachev, Transition between Electron Localization and Antilocalization in Graphene, Phys. Rev. Lett. **103**, 226801 (2009).
[60] H. Fröhlich, Superconductivity in metals with incomplete inner shells, J. Phys. C **1**, 544 (1968).
[61] *Quantum Information and Coherence*, edited by E. Andersson and P. Öhberg (Springer, New York, 2014).